Video Article

A Test Bed to Examine Helmet Fit and Retention and Biomechanical Measures of Head and Neck Injury in Simulated Impact

Henry Y. Yu[1], Brooklynn M. Knowles[1], Christopher R. Dennison[1]

[1]Department of Mechanical Engineering, University of Alberta

Correspondence to: Christopher R. Dennison at cdenniso@ualberta.ca

URL: https://www.jove.com/video/56288
DOI: doi:10.3791/56288

Keywords: Bioengineering, Issue 127, Biomechanics, head injury, neck injury, brain injury, helmet, helmet fit, bicycle, injury prevention, motion capture, impact, trauma

Date Published: 9/21/2017

Citation: Yu, H.Y., Knowles, B.M., Dennison, C.R. A Test Bed to Examine Helmet Fit and Retention and Biomechanical Measures of Head and Neck Injury in Simulated Impact. *J. Vis. Exp.* (127), e56288, doi:10.3791/56288 (2017).

Abstract

Conventional wisdom and the language in international helmet testing and certification standards suggest that appropriate helmet fit and retention during an impact are important factors in protecting the helmet wearer from impact-induced injury. This manuscript aims to investigate impact-induced injury mechanisms in different helmet fit scenarios through analysis of simulated helmeted impacts with an anthropometric test device (ATD), an array of headform acceleration transducers and neck force/moment transducers, a dual high speed camera system, and helmet-fit force sensors developed in our research group based on Bragg gratings in optical fiber. To simulate impacts, an instrumented headform and flexible neck fall along a linear guide rail onto an anvil. The test bed allows simulation of head impact at speeds up to 8.3 m/s, onto impact surfaces that are both flat and angled. The headform is fit with a crash helmet and several fit scenarios can be simulated by making context specific adjustments to the helmet position index and/or helmet size. To quantify helmet retention, the movement of the helmet on the head is quantified using post-hoc image analysis. To quantify head and neck injury potential, biomechanical measures based on headform acceleration and neck force/moment are measured. These biomechanical measures, through comparison with established human tolerance curves, can estimate the risk of severe life threatening and/or mild diffuse brain injury and osteoligamentous neck injury. To our knowledge, the presented test-bed is the first developed specifically to assess biomechanical effects on head and neck injury relative to helmet fit and retention.

Video Link

The video component of this article can be found at https://www.jove.com/video/56288/

Introduction

Most epidemiological evidence suggests bicycle helmets provide protection against head injuries for cyclists of all ages[1]. The biomechanical literature presents the consistent theme that the helmeted head sustains relatively less severe head/brain injuries secondary to impact, relative to the unprotected (un-helmeted) head[2]. Some research suggests that poor helmet fit is associated with an increased risk of head injury[3], implying that helmets are most effective when fit properly. Depending on the criteria used to define good helmet fit, incorrect helmet use was found to be as high as 64% among helmeted cyclists[3]. Despite epidemiological evidence suggesting that helmet fit is relevant in the severity or likelihood of head injury in an impact, there is minimal experimental work assessing in a controlled laboratory setting whether or not correct helmet fit or helmet retention has a significant effect on biomechanical measures of injury. One related study investigates the effect of motorcycle helmet sizing during helmeted impacts simulated with a finite element model[4]. Another related study investigates the effect of helmet sizing during experimental impacts[5] while using pressure sensitive film to quantify fit forces in football helmets. The effect of retention systems in bicycle and motorcycle helmet impacts have been investigated[6,7], as well as a backward fit scenario for preadolescents[6].

Our work proposes methods to study the effect of bicycle helmet fit on the risk of injury with helmet fit force sensors, simulated impacts with an anthropometric head and neck, and stereoscopic high-speed cameras. The goals of our proposed methods are to quantify fit and evaluate the risk of injury in different realistic impact scenarios. In contrast to related methods, our work investigates bicycle helmet fit, where proper helmet use is varied. Similar to previous methods, head kinematics are determined; however, neck loading and head-helmet displacements are also quantified. Although the epidemiology of neck injury in cycling suggests that neck injuries are uncommon, they tend to be associated with more severe head impacts and hospitalization[8,9]. The evidence is mixed on whether or not helmet use reduces rates of neck injury[8] and none of the cited epidemiological studies quantify aspects of helmet fit. Considering the fact that neck injury in cycling tends to be associated with more severe accidents and that helmet fit has not been examined in neck injury epidemiology, methods for examining both head and neck injury are valuable in biomechanical research. Such experimental methods could be used in biomechanical studies that complement epidemiological studies which cannot in all cases control for impact severity or helmet fit.

In our work, a novel method of monitoring relative motions between the head and helmet during impact has been developed. The ability to monitor whether or not the helmet moves on the head can give valuable insight into both helmet stability and exposure of the unprotected head

Copyright © 2017 Journal of Visualized Experiments

to injury during impact. In a study investigating helmet fit, helmet stability and head exposure are particularly valuable in evaluating helmet performance. In contrast to related work, different impact and fit scenarios emphasizing varied helmet positioning will also be tested.

Currently, correct helmet fit is subjective and nonspecifically defined. Generally, good helmet fit is characterized by stability and position. The helmet should be resistant to movement once secured on the head, and should be positioned such that the eyebrows are not covered and the forehead is not excessively exposed. Furthermore, approximately one-finger width of space should fit between the chin and chinstrap[3]. Measures of quantifying helmet fit are not widespread; other than force, methods may compare helmet fit based on comparing head and helmet geometry. One such method is the Helmet Fit Index proposed by Ellena *et al.*[10]. Our proposed method of quantifying helmet fit, fit force sensors, creates an objective means of comparing different helmet fit scenarios in the form of average and standard deviation of forces exerted on the head. These fit force values represent the tightness of a helmet, as well as the variation of tightness experienced on the head. These sensors provide a quantified comparison of forces that can be made between different fit scenarios. A secure tight fitting helmet would show higher forces while a loose helmet would show lower forces. This method of fit force measurement is similar to the Average Fit Index proposed by Jadischke[5]. However, Jadischke's methods utilize pressure sensitive film. The optical sensors we present allow unobtrusive measurement of fit force around the head or helmet.

For certification of helmets, a helmet is secured on an instrumented headform, which is then raised to a certain height to be dropped. The head and helmet is then subject to a free fall drop onto an anvil while recording linear accelerations. Although not typically used in helmet industry standards, a Hybrid III head (headform) and neck assembly were used in this work, with a guided drop tower to simulate impacts. In contrast to standards that typically use linear kinematics, the headform accelerometer array also allows the determination of rotational kinematics, a key parameter in predicting the likelihood of diffuse brain injuries, including concussion[11]. Through measurement of both linear acceleration and rotational acceleration and velocity, estimates of severe focal and diffuse head injury can be made by comparing kinematics to the several proposed kinematics-based injury assessment methods in the literature[12,13]. While the headform was originally developed for automotive crash testing, its use in helmet assessment and estimation of head injury risk in helmeted impact is well documented[2,14]. The impact simulation setup also includes an upper neck load cell, allowing the forces and moments associated with neck injury to be measured. Neck injury risk can then be estimated by comparing neck kinetics to injury assessment data from automotive injury data[12,13].

A method of tracking helmet movement relative to the head during impact with high speed video is also proposed. Currently, no quantitative methods exist to evaluate helmet stability during impact. The Consumer Product Safety Commission (CPSC)[15] bicycle helmet standard calls for a positional stability test, but is not representative of an impact. Furthermore, whether or not the helmet comes off the headform is the only result measured by the test. Regardless of exposure of the head to injury, a helmet may still pass as long as it stays on the headform during tests. The proposed method of tracking helmet movement is similar to Helmet Position Index (HPI)[15] and measures the distance between the brim of a helmet and the forehead. This head-helmet displacement is tracked using high-speed video footage throughout an impact in order to obtain a representation of helmet stability and head exposure during impact. Using Direct Linear Transform (DLT)[16] and Single Value Decomposition (SVD)[17] methods, markers are tracked from two cameras to determine point locations in three-dimensional space and then the relative displacement between helmet and head.

Several impact severity and fit parameters are investigated. The impact scenarios include two impact speeds, two impacting anvil surfaces, and both torso-first and head-first impacts. In addition to a typical flat anvil surface, an angled anvil impact is also simulated to induce a tangential force component. A torso-first impact, as opposed to a head-first impact, is included to simulate a scenario in which a rider's shoulder impacts the ground before the head, similarly performed in previous work[18]. Finally, these four helmet fit scenarios are investigated: a regular fit, an oversized fit, a forward fit, and a backward fit. Unlike previous work, helmet positioning on the head is an investigated parameter, as well as helmet fit and helmet sizing.

Protocol

1. Helmet Fit Scenarios Arrangement

1. Define fit scenarios to be studied on an anthropometric test device head and neck (Hybrid III 50th percentile male) with a head circumference of 575 mm.
   NOTE: An example of four fit scenarios is shown in **Table 1** with helmet positions corresponding to **Figure 1**. The forward and backward fit scenarios were based on definitions of correct helmet use from previous epidemiological studies, which specified proper helmet position as not covering the eyebrows or exposing the forehead[3].
2. For each scenario, mark each helmet position on the headform to ensure the helmet fit scenario is consistently repeated.
3. **Use a CPSC certified helmet, available in universal and extra-large sizes, for all fit scenarios.**
   NOTE: According to the manufacturer provided fit guide, a universal size most appropriately fits the headform circumference.
   1. For each fit scenario, keep other fit parameters consistent. Specifically, tighten the chinstrap to leave approximately one finger width of space under the chin and hand-tighten the adjustable dial to maintain a secure fit.

2. Fit Force Measurement

1. Arrange five fit sensors on the skin of the headform, positioned on the front, back, left, right and top (**Figure 2**).
   NOTE: The sensors are a modified version of Bragg grating force transducers developed within the research group[19,20,21,22], optimized to measure fit forces over a range of 0 to 50 N. The modified sensors have a thickness and diameter of 2.6 mm and 14 mm respectively.
2. Take a reference measurement with the transducers on the un-helmeted headform under no load. Take this reference measurement prior to each fit force measurement.
3. Place the helmet onto the headform and measure force data for 3 s at a rate of 2.5 kHz. Repeat the same fit scenario six times for repeated measurements.

4. Repeat the same measurement procedure for all fit scenarios.
5. Convert wavelength shift data to force measurements by multiplying the measured wavelengths from the transducer by the pre-determined calibration constant for the fit force transducer.

3. Drop Tower for Impact Simulation

1. **Simulate impact to the helmeted head by linearly guiding the headform to hit an impact surface[19,23]. The equipment required to do this is context specific, as detailed below.**
    1. Assemble a drop tower to consist of an adjustable drop gimbal, an anthropometric test device head and neck, and a variable impact surface.
    NOTE: The total drop assembly mass is approximately 11 kg. The added mass of the gimbal accounts for the exclusion of the full human body as an effective torso mass to better simulate a realistic impact[24].
    2. Arrange 9 uni-axial accelerometers in a 3-2-2-2 configuration within the headform to allow linear and angular accelerations of the headform to be determined at the center of gravity[25].
    3. Arrange a purpose built velocity gate on the impact tower to measure impact velocity immediately before impact.

2. Collect head acceleration and neck force/moment data using the data acquisition system. Filter analog voltages, sampled at 100 kHz for all channels. Prior to the data acquisition system, include a hardware anti-aliasing low pass filter with a corner frequency of 4 kHz[26].
3. **Arrange the impact scenario.**
    1. For all impacts, remove the helmet visor to allow for better visibility during motion tracking. The effect of the visor during impact is assumed to be negligible due to its loose attachment.
    2. Arrange all drops to impact the forehead. This is a common impact location in cycling[27], although other scenarios could also be simulated.
    3. Simulate six different impact scenarios by varying impact speed, impact surface, and either head-first or torso-first impacts as per **Table 2**.
    4. Raise the headform to the appropriate height, corresponding to specified impact velocities. Drop the headform from an appropriate height, typically 0.82 m and 1.83 m, to achieve velocities of 4 m/s and 6 m/s, respectively.
    NOTE: Add height as necessary to overcome friction losses. Two impact velocities of 4 m/s and 6 m/s can be chosen based off previous literature and standards[28].
    5. Arrange the impact surface.
        1. Arrange either a flat or a 45° angled anvil (**Figure 4**). The flat anvil simulates falls on a flat surface, while the angled anvil simulates impacts with a tangential velocity component.
        2. Cover both of the surfaces of the anvils in abrasive tape to simulate an asphalt surface. Adjust the anvil position as necessary between impacts to ensure the helmet to be impacted contacts only the flat surface of the anvil.

4. **Arrange the drop tower for either head-first or torso-first impact. Simulate both head-first and torso-first impacts, with torso impacts similar to the combined loading impact configuration presented in Smith *et al.*[18]**
    1. To simulate a head-first impact, do not adjust the drop tower.
    2. To simulate the torso hitting the ground before the head, place a wooden block in the path of the drop gimbal. Place this wooden block at a height such that the head is approximately 25 mm away from impacting the anvil at the torso-impact. The head will then continue to hit the anvil by means of neck flexion only.
    3. Include a layer of foam to minimize vibrations from the drop tower (**Figure 5**).
    4. In contrast to head-first impacts, adjust the angle of the neck in torso-first impacts.
    NOTE: This neck angle adjustment allows for the head to impact the anvil on the forehead after flexion, so that impact location is comparable to the head-first impact case (**Figure 6**). In addition to forehead impacts, this torso-first scenario would certainly be relevant in side impacts as well. In both head-first and torso-first impacts, this gimbal system allows for movement of the head and neck along the track after impact.

5. **Trigger the data acquisition system, high speed cameras (see section 4), and drop of the headform simultaneously. Repeat the same impact and fit scenario configuration 3 times with new helmets each time.**
NOTE: The high-speed cameras will need to be set up concurrently with the drop tower, detailed in section 4.
6. Subject each of the four fit scenarios to each of the 6 different impact scenarios. Perform a total of 72 drops after 3 trials of each configuration.
7. **Post-process the headform kinematic and kinetic data.**
    1. Filter analog signals for acceleration and force/moment subsequently using a 4th order Butterworth filter in post processing to meet industry suggested practice[26]. Filter head accelerations and neck forces as per Channel Frequency Class (CFC) 1000. Filter neck moments as per CFC 600.

4. Motion Capture Using a High Speed Dual Camera System

NOTE: Recording marker positions from two high speed cameras allow three-dimensional marker positions to be determined with the DLT method[16] in post-processing. To determine head-helmet displacements, track markers on both the headform and helmet during impact.

1. **Arrange high-speed cameras around the drop tower.**
    1. Arrange two high-speed cameras around the drop tower to capture synchronized images of the helmet and headform movement during impact.

1. Place a master camera to the side of the drop tower and place a slave camera at approximately 45° from the master (**Figure 7**). Setup a 250 W light between the cameras to allow for sufficient exposure.

2. **Configure high speed cameras.**
   1. Equip each camera with either a 50 mm f/1.4 or 100 mm f/2.0 macro lens, depending on the field of view required. Set the apertures on the lenses at f/8.0.
      NOTE: This aperture allows for sufficiently sharp focus in the desired depth of field. The required field of view ranged from 30-60 cm, depending on the impact scenario.
   2. Configure both cameras to record at 1280 x 800 pixels at a frame rate of 1000 frames per second or faster. Thus, the maximum exposure time per frame will be 600 µs.
   3. Synchronize the two cameras in frames and internal clock. Set up a trigger so that both cameras trigger simultaneously.

3. **Calibrate the space by taking a still image of a calibration frame from each camera.**
   NOTE: For the direct linear transformation (DLT) method, the space must be initially calibrated.
   1. Move a calibration cage with 17 known calibration point locations into the field of view of both cameras and take a single image from each camera. A minimum of 11 common points must be visible from both cameras.
   2. Find the two-dimensional coordinates of each marker with tracking software.
      NOTE: A coordinate measuring machine (CMM) determines the point locations of the calibration cage prior to DLT calibration.
   3. Using a series of calculations performed with the calibration markers' coordinates (known as DLT)[16], transform any two dimensional marker locations into three-dimensional coordinates relative to the calibration cage coordinate system in post-processing.

4. To quantify helmet displacement, track the distance between a point on the headform forehead and the brim of the helmet using the tracking software.
   NOTE: Because these points are not visible from both cameras, track a set of three visible markers on each the headform and helmet instead. The points on the forehead and helmet can then be indirectly tracked.
5. **Place motion tracking markers on the headform and take a still reference image of the headform from each camera.**
   1. For this method of indirect marker tracking, take a headform reference image with each camera. Ensure that this reference image consists of three markers and a reference marker defined on the head.
   2. Maximize the distance between markers using three reference point locations while remaining in both cameras' field of views.
      NOTE: Maximizing the distance allows for better accuracy by decreasing indirect marker tracking sensitivity to tracking errors. The three markers allow for the three-dimensional reconstruction of motion in post processing, as well as the estimation of the forehead location.
   3. Hold the reference marker between the eyes on the lower forehead and the other markers spread across the headform. Ensure that these three other markers are visible from both cameras throughout an impact (**Figure 8**).

6. **Place motion tracking markers on the helmet and take still reference images of the helmet from each camera as described for the headform reference (section 4.5).**
   1. Ensure that the reference consists of viewing at least four motion tracking markers. Hold one marker on the bottom of the helmet brim as a reference and spread the other three markers on the helmet. Ensure that these three markers are visible from both cameras throughout an impact. Take a single image from each camera for the helmet reference (**Figure 9**).

7. **Trigger the data acquisition system, high speed cameras, and drop of the headform simultaneously as described in section 3.**
   NOTE: The drop tower will need to be set up concurrently with the high-speed cameras. After taking reference images, a drop may be performed.
   1. Arrange the helmet fit scenario. Record the drop. Signal a trigger to the cameras manually upon impact. Arrange recording so that 3 s is recorded prior to the trigger and 8 s is recorded after the trigger. Manually review and bracket the synchronized camera images to contain the impact only.

5. Head-helmet Marker Tracking and Post-processing

1. **Track head and helmet markers throughout the impact, using camera-specific software.**
   1. Track six points per drop: three on both the helmet and headform (**Figure 10**). With the software, determine the transient two-dimensional pixel coordinates of each marker.

2. Use the DLT method to calculate three-dimensional coordinates of tracked markers during a drop.
   NOTE: With the calibration data from the calibration cage and the drop data from the two cameras, the DLT method can determine the three-dimensional coordinates of the tracked markers during a drop.
3. **Use the SVD (singular value decomposition) method[17] to calculate the 3-D dimensional coordinates of the headform forehead and helmet brim. The difference between these two points is head-helmet displacement.**
   1. Use the SVD method to estimate the location of a reference point on each the headform forehead and helmet brim from the tracked markers.
   2. Use the SVD method to find the transformation matrix of the three markers between the reference frame and each individual frame of a drop. This transformation can be applied to find either the forehead or helmet brim locations.

4. Perform this indirect tracking on both the helmet and headform. The displacement between the forehead and helmet brim can then be monitored (**Figure 11**).

Representative Results

Fit Force Measurement

For each fit scenario, fit force measurement was performed at each sensor location (**Figure 12**) and a t-test, assuming unequal variances, was performed to determine significance ($p < 0.05$). The average standard deviation across all measurements was ± 0.14 N. Higher fit forces indicate a tighter fit.

Head Kinematic and Neck Kinetic Data

The resultant head linear acceleration, head angular acceleration, head angular velocity, upper neck force, and upper neck moment from a typical drop are shown (**Figure 13** through **Figure 17**). Resultant values were computed by taking the absolute norm of the *x*, *y*, and *z*, direction vectors (**Figure 3**). A neck injury criterion computed from neck axial force and moment[13], N_{ij}, was also computed throughout the impact (**Figure 18**). From the kinematic results, the different events of the impact can also be identified. For instance, head contact with the anvil in the torso-first impacts can be observed as the large peak in resultant linear acceleration (**Figure 13**). In angular acceleration, two sets of peaks could be observed (**Figure 14**). The first peak occurs as a result of the torso impact while the second peak occurs as a result of the neck reaching maximum flexion. In sequence, the events of the impact are torso impact, followed by head contact with the anvil, and then the neck reaching maximum flexion. These events can also be observed in high speed video (**Figure 6**).

Head-Helmet Relative Motion

The magnitude of the vector between the forehead and helmet brim, indicating relative head-helmet motion, is shown in **Figure 19** for two fit scenarios. Relative change in displacement can be an indicator of helmet movement relative to its pre-impact location.

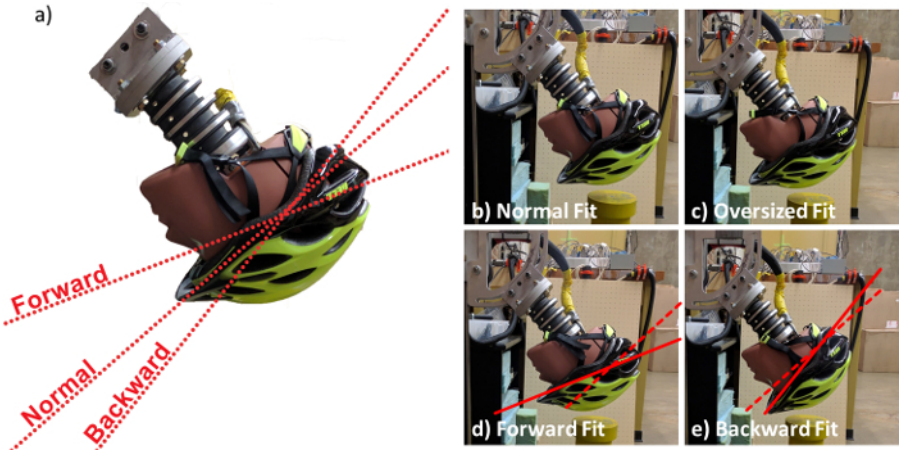

Figure 1: Helmet fit scenarios. Helmet Fit Scenario Comparisons on the headform showing (**a**) Comparison between normal fit and improperly positioned fits (**b**) normal fit scenario (**c**) oversized fit scenario (**d**) forward fit scenario (**e**) backward fit scenario. Please click here to view a larger version of this figure.

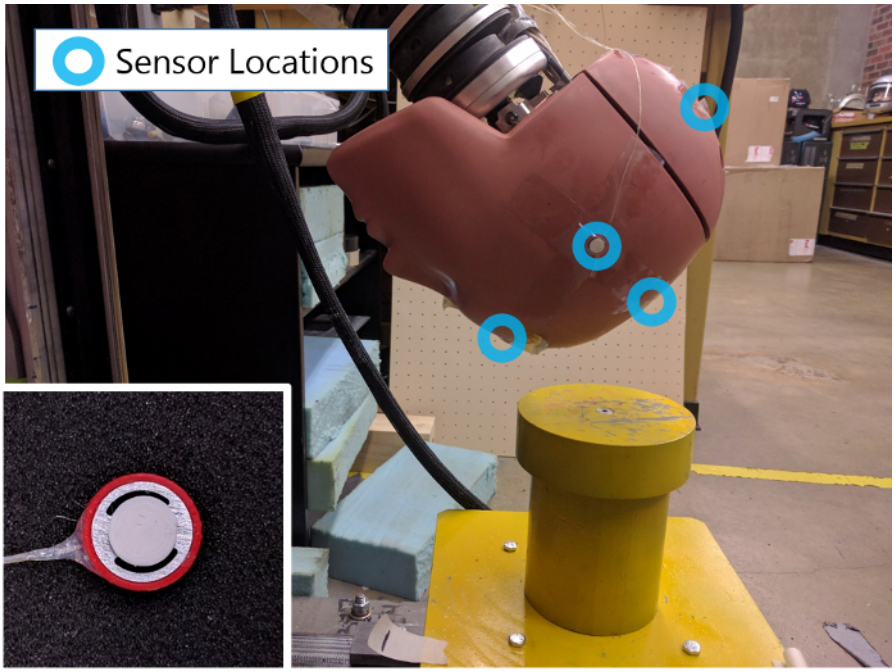

Figure 2: Fiber Bragg grating (FBG) five sensor array on headform with sensor located on the front, back, left, right, and top. Each sensor (bottom left) has a thickness and diameter of 2.6 mm and 14 mm, respectively. Please click here to view a larger version of this figure.

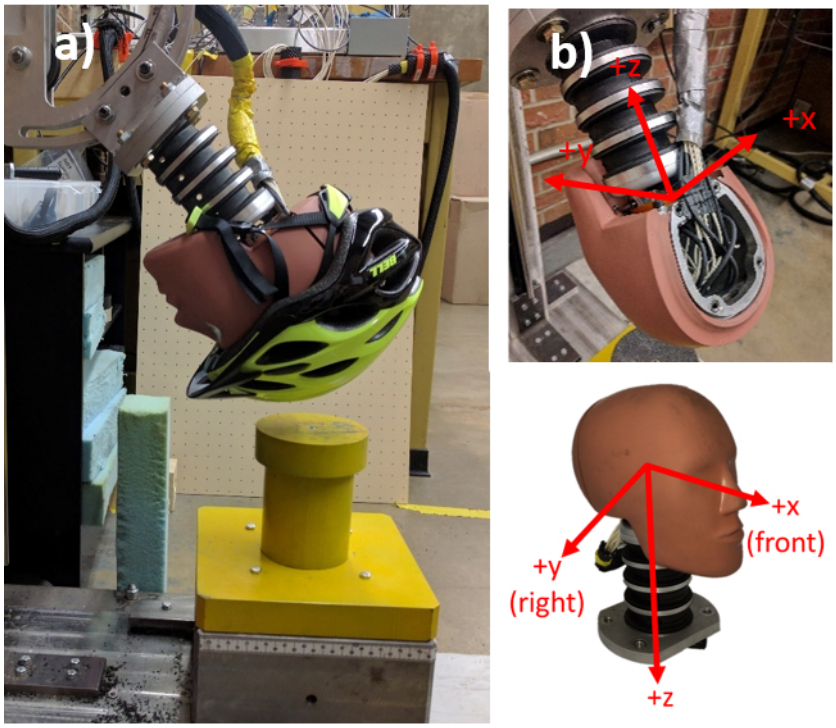

Figure 3: Drop tower assembly with associated coordinate axis. (**a**) Overall Drop Tower Assembly with helmeted headform (**b**) Instrumented headform and neck load cell. Neck load cell coordinate axis is also shown. (**c**) Corresponding head coordinate axis. Head accelerations and neck loads are measured with reference to the coordinate axis shown, with positive magnitudes in the axis directions. Moments are based on the right hand rule.

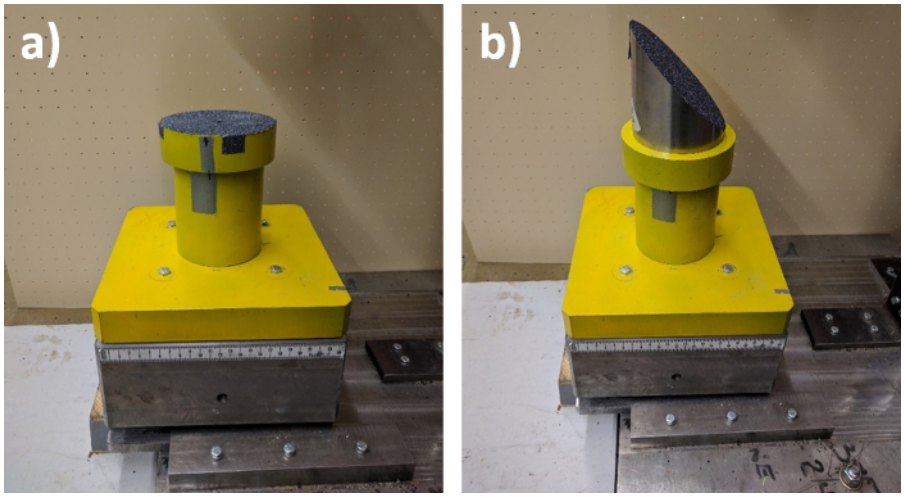

Figure 4: Interchangeable (**a**) flat and (**b**) 45° angled anvil surfaces covered in abrasive tape. Please click here to view a larger version of this figure.

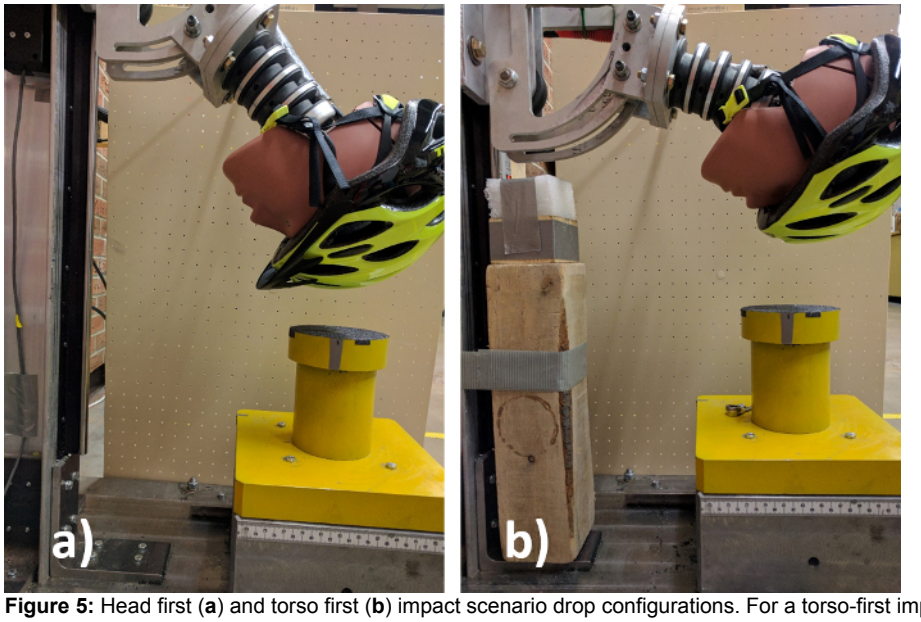

Figure 5: Head first (**a**) and torso first (**b**) impact scenario drop configurations. For a torso-first impact scenario, a wooden block is used to stop the drop assembly to simulate a torso impact. The helmet visor was also removed prior to all impact simulations. Please click here to view a larger version of this figure.

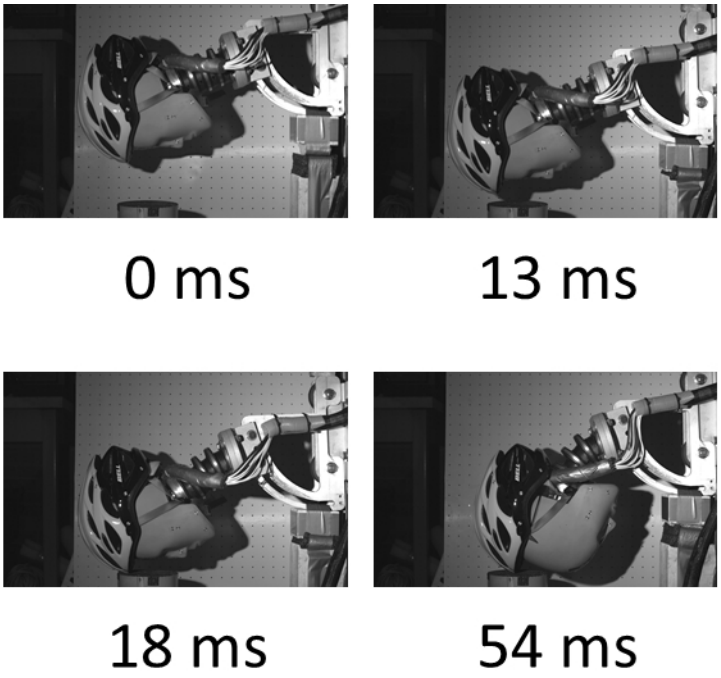

Figure 6: Sequence of images in a torso-first impact. In a torso first impact, the drop gimbal is stopped, allowing for the head to impact the anvil, followed by neck flexion. In contrast, a head-first impact allows full linear movement of the drop gimbal for the head to contact the anvil first.

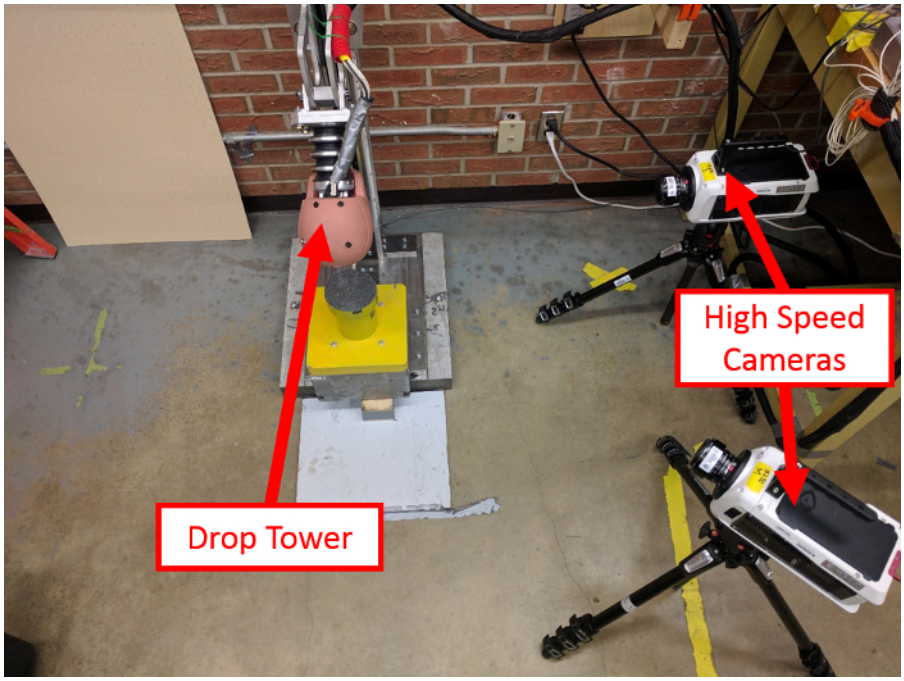

Figure 7: Dual high-speed camera arrangement around drop tower. Please click here to view a larger version of this figure.

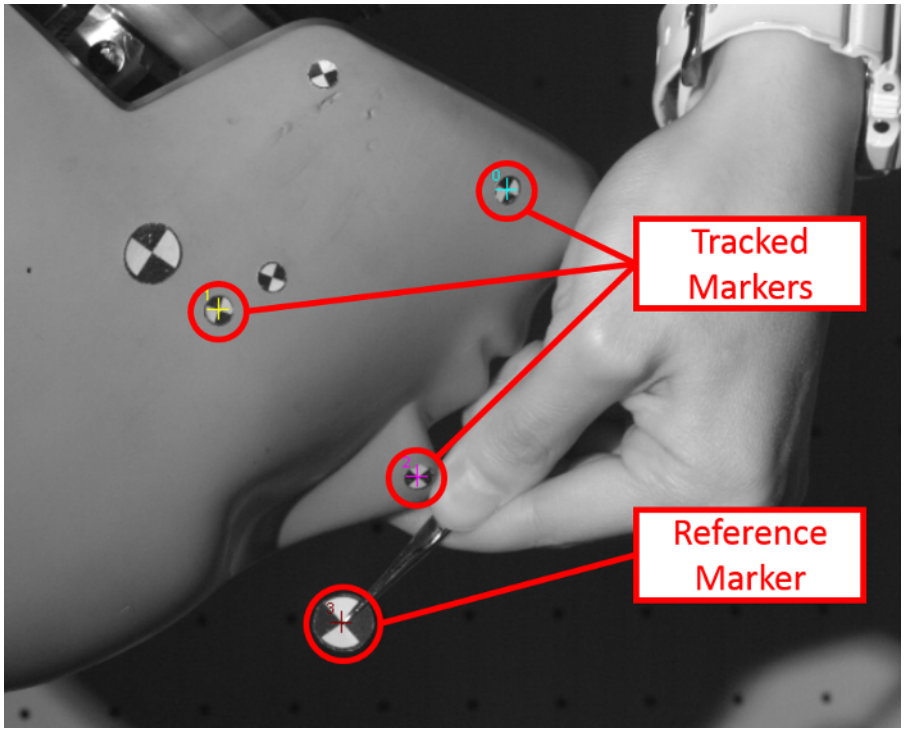

Figure 8: Head reference image markers for motion tracking. Three markers on the head are tracked during impact while a fourth marker defines the forehead point used to calculate head-helmet displacement. Please click here to view a larger version of this figure.

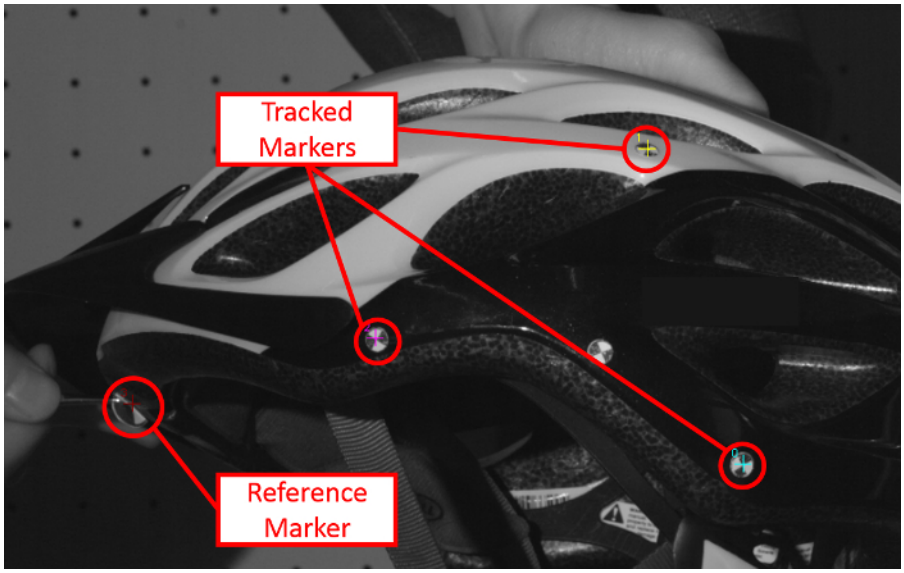

Figure 9: Helmet reference image markers for motion tracking. Three markers on the helmet are tracked during impact while a fourth marker defines the helmet brim point used to calculate head-helmet displacement. Please click here to view a larger version of this figure.

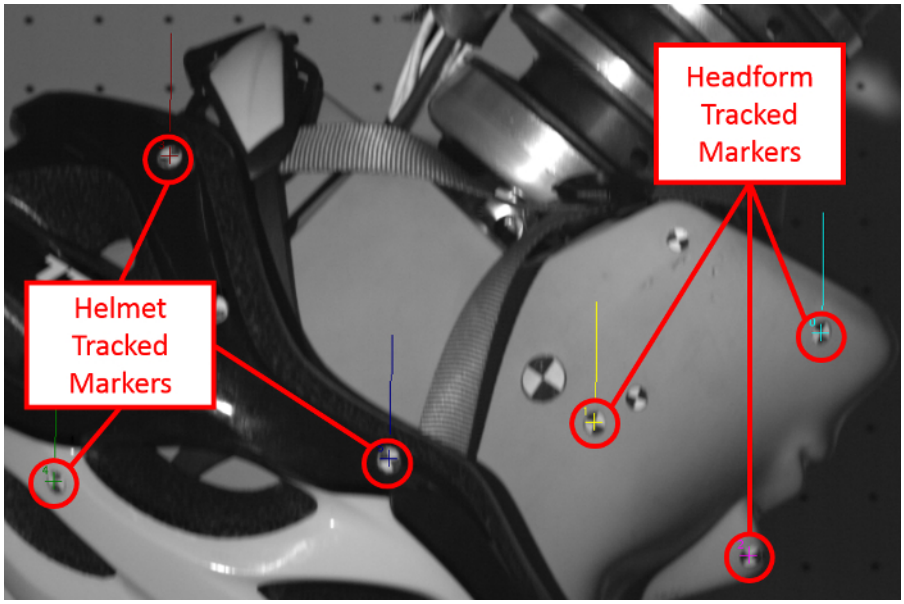

Figure 10: Tracked markers during impact. Three markers are tracked on both the headform and helmet. Please click here to view a larger version of this figure.

Figure 11: Head-helmet displacement vector between forehead and helmet brim that is tracked throughout impact.

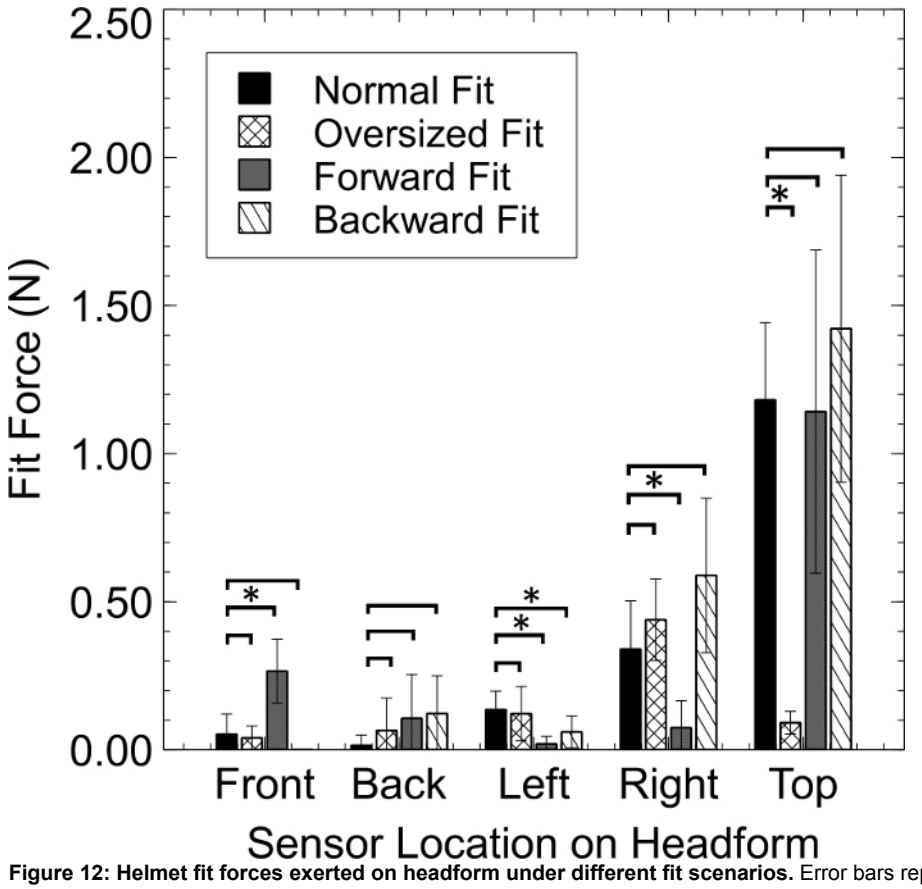

Figure 12: Helmet fit forces exerted on headform under different fit scenarios. Error bars representing standard deviation are also shown. Significant differences ($p < 0.05$) between fit force scenarios are indicated (*). Please click here to view a larger version of this figure.

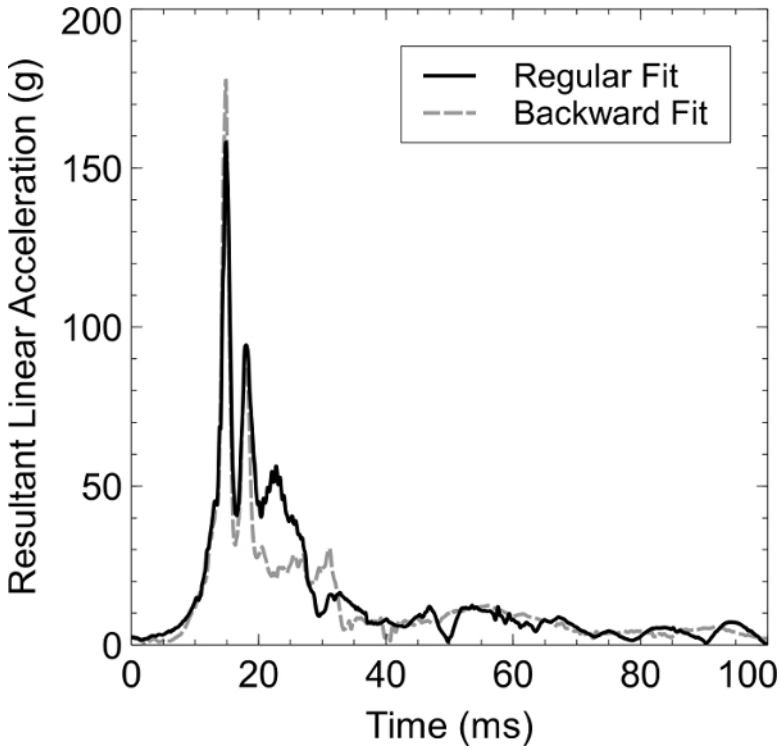

Figure 13: Resultant head center of gravity (COG) linear acceleration for a torso first-impact onto a flat anvil at 6 m/s. A regular fit (solid line) and backward fit (dotted line) scenario are compared. Please click here to view a larger version of this figure.

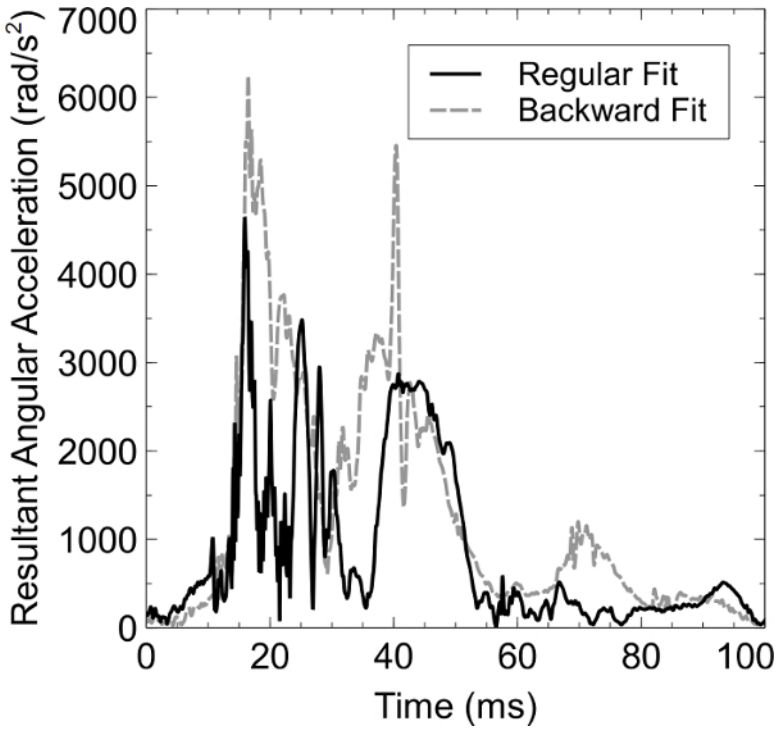

Figure 14: Resultant head center of gravity (COG) angular acceleration for a torso first-impact onto a flat anvil at 6 m/s. A regular fit (solid line) and backward fit (dotted line) scenario are compared. Please click here to view a larger version of this figure.

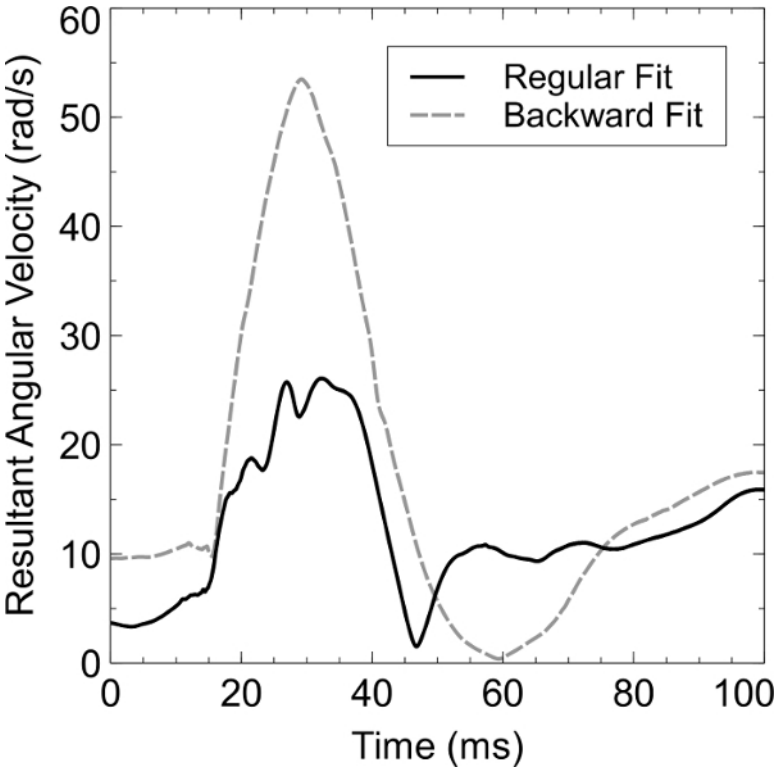

Figure 15: Resultant head center of gravity (COG) angular velocity for a torso first-impact onto a flat anvil at 6 m/s. A regular fit (solid line) and backward fit (dotted line) scenario are compared. Please click here to view a larger version of this figure.

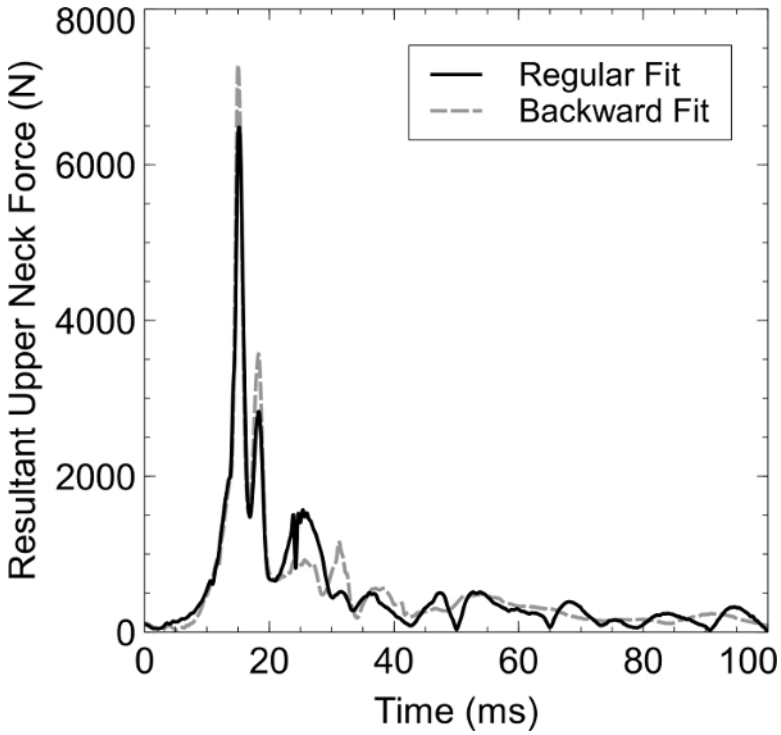

Figure 16: Resultant upper neck force for a torso first-impact onto a flat anvil at 6 m/s. A regular fit (solid line) and backward fit (dotted line) scenario are compared. Please click here to view a larger version of this figure.

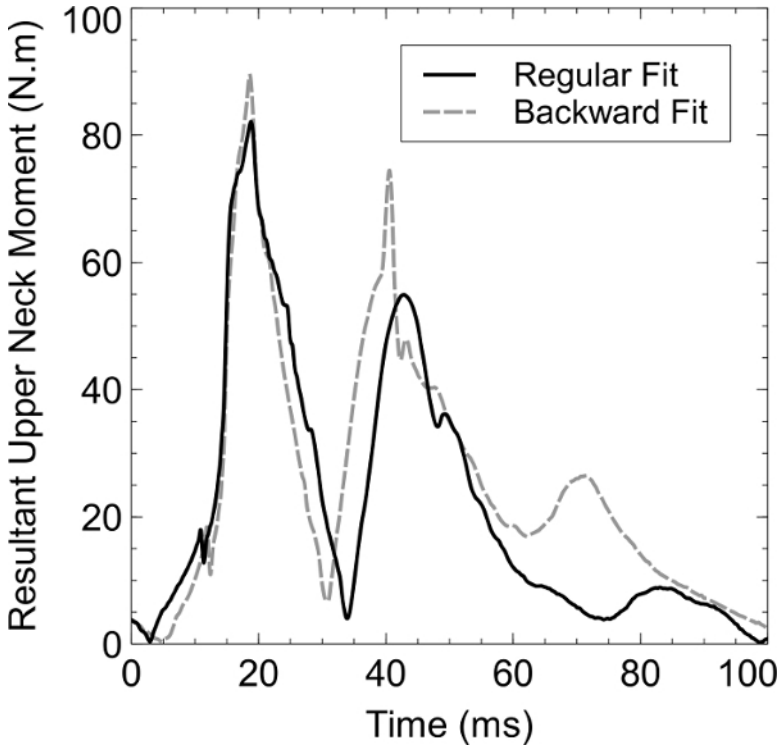

Figure 17: Resultant upper neck moment for a torso first-impact onto a flat anvil at 6 m/s. A regular fit (solid line) and backward fit (dotted line) scenario are compared. Please click here to view a larger version of this figure.

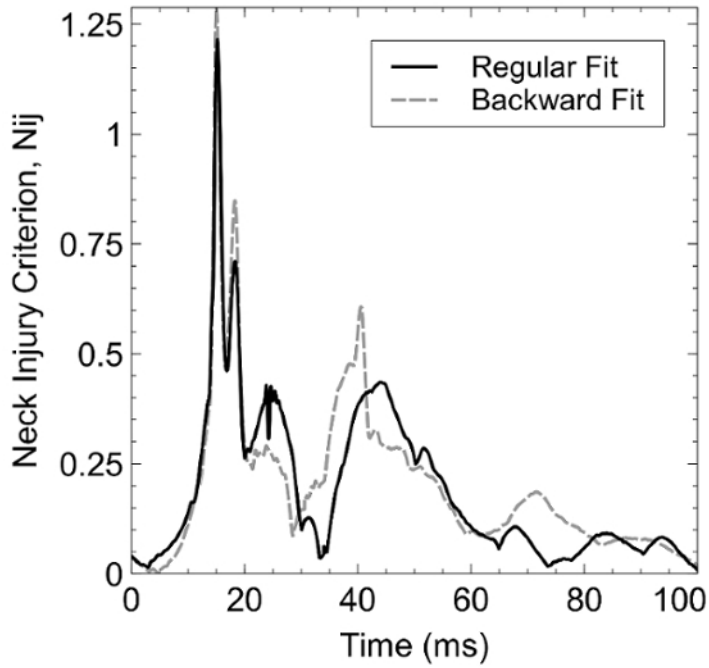

Figure 18: N_{ij} for a torso first-impact onto a flat anvil at 6 m/s. A regular fit (solid line) and backward fit (dotted line) scenario are compared. Please click here to view a larger version of this figure.

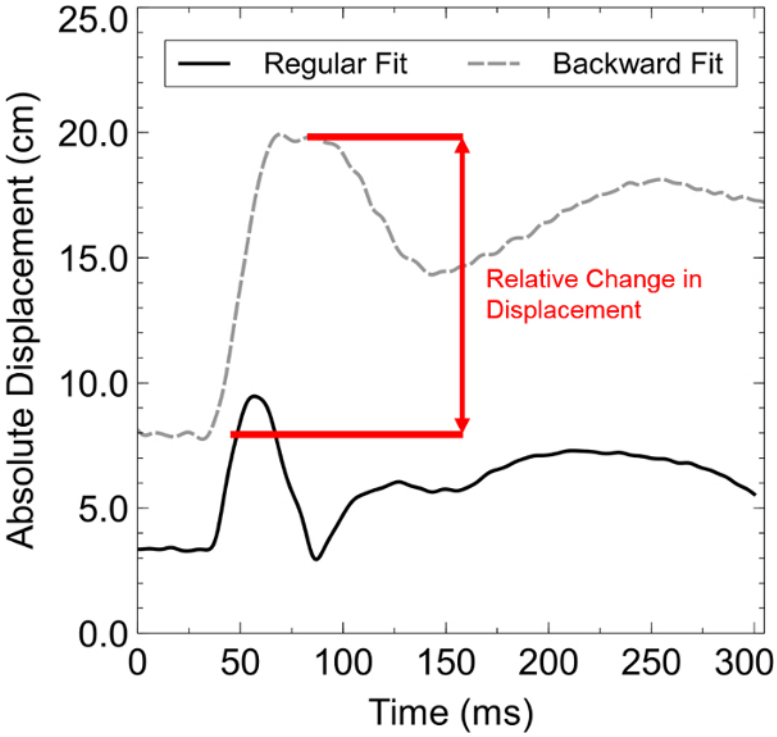

Figure 19: Transient head-helmet displacement for a torso first-impact onto a flat anvil at 6 m/s. A regular fit (solid line) and backward fit (dotted line) scenario are compared. The relative change in displacement, in contrast to absolute displacement, is also shown. Please click here to view a larger version of this figure.

Fit Scenario	Helmet Size	Helmet Position
Normal (**Figure 1b**)	Universal	Normal
Oversized (**Figure 1c**)	XL	Normal
Forward (**Figure 1d**)	Universal	Forward
Backward (**Figure 1e**)	Universal	Backward

Table 1: Helmet Fit Scenarios to be studied. The fit scenarios are based on definitions of correct helmet use from previous epidemiological studies specifying proper helmet position[3].

Impact Scenario	Impact Speed	Impact Surface	Head/Torso First
1	Low (4 m/s)	Flat	Head
2	High (6 m/s)	Flat	Head
3	Low	Angled	Head
4	High	Angled	Head
5	Low	Flat	Torso
6	High	Flat	Torso

Table 2: Impact Scenarios to be simulated.

Discussion

Here, methods for investigating helmet fit in simulated helmeted head impacts are presented. Helmet fit was quantified with fit force sensors, impacts were simulated with an ATD headform and neck on a guided drop tower, and helmet movement was tracked with high speed video. Different impact scenarios were simulated under different fit scenarios to investigate the effects on biomechanical measures of helmet fit.

The helmet fit sensors are capable of distinguishing differences in fit forces between different helmet fit scenarios (**Figure 12**). Trends in fit forces between different fit scenarios do not strongly correlate with helmet performance. A helmet fit with poor stability (*e.g.* backward fit, as shown in **Figure 1**) is expected to exhibit significantly lower fit forces. Despite increased amounts of helmet movement (backward fit, **Figure 19**), a backward fit helmet exhibits significantly lower fit forces at only one sensor location when compared to a regular fit. This result suggests that helmet tightness on the head may not be the sole determinant of fit that guarantees dynamic stability of the helmet on the head. In this study, the fit forces were measured with the head inverted. The forces could have also been measured with the head in a right side up position, which would result in higher measured forces at the head vertex than reported in this study. However, the protocol of comparing fit forces between different fit scenarios seeks to quantify relative changes in fit force. Regardless of whether the head is upright or inverted, the relative changes in forces are the same.

The test bed and presented methods are capable of determining linear and angular kinematics including acceleration and velocity as well as neck forces and moments over the impact duration. Contemporary biomechanical injury measures are based on impact kinematics and time duration. For example, the head injury criterion (HIC) integrates linear acceleration over time[12], while the brain injury criterion (BrIC) is based on peak angular velocity[11]. Other kinematic-based injury measures include the generalized acceleration model for brain injury threshold (GAMBIT)[29], based on peak linear acceleration and peak angular acceleration, and the head impact power (HIP), which includes linear and angular acceleration, time duration, and directional considerations[30]. Alternatively, neck forces and moments are used to compute neck injury criterion N_{ij}[12]. As this experimental protocol is capable of measuring all relevant kinematics and kinetics, it is possible to compute any biomechanical injury measures that are of interest. Potential injury risk can then be determined based on the literature associated with each injury measure. As a result, the setup proved capable of detecting alterations in biomechanical measures of head and neck injury based on helmet fit. Therefore, the test bed can be used to study fit and retention and their relation to focal and diffuse head injury and osteoligamentous neck injury. For example, in a torso-first impact onto a flat anvil at 6 m/s, a regular fit and backward fit scenario were compared. For the regular fit scenario, peak resultant linear accelerations, peak angular accelerations, and change in angular velocities were 158.2 g, 4647.5 rad/s^2, and 22.39 rad/s respectively. Compared to the regular fit, a backward fit scenario exhibited higher values of 177.9 g, 6246.4 rad/s^2 and 45.91 rad/s, suggesting a higher risk of head injury (**Figure 13** through **Figure 17**) with t-test p-values of 0.012, 0.070, and 0.005, respectively. Because integration of noise in angular acceleration created an offset in angular velocity, the change in angular velocity is reported instead to account for this offset. For the same impact scenario, the Neck Injury Criterion (N_{ij}) was determined from neck force and moment. For a regular helmet fit scenario, a peak N_{ij} of 1.23 was determined, while a backward helmet fit measured 1.28 (**Figure 18**) with a t-test p-value of 0.099. Again, a higher value of N_{ij} would suggest a greater risk of neck injury.

The high speed video analysis techniques proved capable of detecting alterations in dynamic stability and retention. For the same torso-first impact onto a flat anvil at 6 m/s, a regular fit and backward fit scenario were compared in terms of helmet displacements. The regular fit scenario experienced a maximum change in head-helmet displacement of 6.52 cm while the backward fit scenario experienced 12.18 cm (**Figure 19**) with a t-test p-value of 0.006. With nearly twice as much helmet movement, these trends suggest that a backward fit scenario results in increased head exposure and, perhaps, greater exposure to forehead injury in a subsequent impact following the first.

Absolute displacement and relative displacement (**Figure 19**) convey the amount of facial and forehead exposure and head-helmet relative motion, respectively, both of which are important when examining retention and dynamic stability. The proposed method of tracking helmet displacements relative to the head allows head exposure and helmet stability during impact to be represented and can evaluate helmet retention for subsequent impacts. The method can show helmet movement throughout an impact, which can be characterized as absolute displacements

Copyright © 2017 Journal of Visualized Experiments

and changes in displacement (**Figure 19**). A poorly retained helmet would exhibit greater displacements, while a well-retained helmet would exhibit lesser displacements. In this study, absolute displacement indicates the amount of facial exposure and relative change in displacement indicates the maximum relative motion between the brow and helmet brim (**Figure 19**). This reported displacement value is determined from the distance between two markers, connected by a single axis. Using the same experimental methods, it would also be possible to measure relative displacement in three component directions to more thoroughly characterize fit and retention. A single component was chosen for simplicity, as well as providing a good comparison to HPI. In other impact conditions, such as side impacts, more component directions or head-helmet rotation could be particularly valuable.

A drawback with the currently proposed sensors and fit force measurement is the limited spatial resolution with which forces are measured. With a 5-sensor array, the distribution of force across the entire helmet may not be fully represented. Because the design of bicycle helmets often includes open vents, a sensor may not always contact the helmet and measure zero force as a result. One potential solution is to place the force sensors on the helmet instead of the head. In the presented protocol, the force sensors were placed on the head to maintain consistency and repeatability of the experiment. Having sensors placed on the helmet could require a different protocol for different helmet types. However, the small size of the sensors and multiplexing ability of Fiber Bragg Grating (FBG) sensors allow a greater number of sensors to be feasibly distributed around the head. Additional sensors could discern the locations of high and low fit force fluctuations and provide further insight on helmet stability. In addition to the magnitude of force in representing tightness, it may also be valuable to consider contact area between the helmet and head. Especially in the case of helmets with open vents, the total contact area or its distribution may be important for characterizing fit. Although changes in overall average tightness were not as apparent in different scenarios of helmet positioning, significant changes in the distribution of forces could be identified, as seen in **Figure 12**.

As with all biomechanical work based on ATDs, there are limitations in the presented methods. Unlike real world impacts, parameters such as impact speed, impact location on the helmet, and impact surfaces are controlled. Therefore, the work presented will not capture the variability of these parameters from cyclist to cyclist and from incident to incident leading to head impact.

The Hybrid III was developed for automotive crash testing, as opposed to helmet research. Unlike a National Operating Committee on Standards for Athletic Equipment (NOCSAE) headform[31], it was not designed for use with a helmet. In contrast, the NOCSAE headform was designed with size and shape specifications based on cadaver heads for an average adult football player and some consider it to more accurately approximate head anthropometry. Because headform geometry has a significant role in studying helmet fit, the headform may have certain shortcomings for different helmet types. In particular, the headform has notable geometrical differences to the NOCSAE head in the base of the skull, cheeks, jaw, and chin[32,33]. Because there is minimal contact between these features and bicycle helmets, shape differences between the headform and an actual head may have minimal influence on head-helmet interaction. Therefore, we argue that the headform is an appropriate model to use in comparative studies between fit scenarios, like that presented here. Any influence due to shape differences would be most apparent in the interface between the retention ratchet system and the bottom ledge of the skull cap, particularly in the backward fit scenario. Related to the headform head, the neck has been criticized for its greater stiffness compared to a human neck, and some hypothesize that the lack of realistic stiffness can contribute to head motions that differ from those of a real human suffering head impact[34]. These effects would be considerably more significant in the torso-first impacts because the trajectory and kinematics of the head are dependent on the neck. For a torso-first impact, an overly stiff neck could attenuate the head's motion after the torso contact and unrealistically slow the head's impact velocity at head contact. With limited existing literature investigating torso-first impacts, the biofidelity of the kinematic traces are difficult to validate with real-world cyclists impacts. However, head angular acceleration from the torso traces are comparable to similar combined loading scenarios performed by Smith *et al.*[18]. As such, the trends in angular acceleration and neck load in different fit scenarios should be emphasized, rather than reported absolute magnitudes. We feel the neck is an appropriate model for the presented study because we compare neck kinetics and head motions between cases of fit and, instead of commenting on absolute magnitudes of head kinematics and neck kinetics, we note changes in these measures.

Another limitation of using the headform in studying helmet fit is the dissimilarity of the headform vinyl skin with that of a human scalp. With practical variations such as hair, oil, and moisture, an accurate simulation of all these variables would be difficult. Although efforts in creating an artificial scalp for helmet research have been pursued[35], validations of head helmet interaction between artificial and human scalps have been minimal. Since it is generally accepted that the headform skin exhibits a higher coefficient of friction than a human scalp, helmet retention could be misleadingly improved. With varying dependence on head-helmet friction in different fit scenarios, the effect of the headform vinyl skin could also be more or less pronounced. For instance, a normal fit scenario may retain a helmet due to head shape while a forward fit may retain a helmet due to the increased head-helmet friction of the vinyl skin. However, the helmet displacements are dependent on the headform scalp in this study. As such, findings should be based on changes and trends between different fit scenarios.

Though four fit scenarios were investigated, more variables exist in characterizing helmet fit. These proposed methods could allow for the study of other helmet fit scenarios, such as more helmet sizes or different levels of ratchet retention tightness. In this study, the ratchet retention system was tightened to a consistent level of tightness, subjective to the researcher. A more realistic tightness could be achieved by measuring the fit forces on volunteers, similar to Jadischke's helmet fitment study[5]. The retention system could then be arranged on the headform and tightened to a level exhibiting the same fit forces. In future work, fit scenarios with different helmet sizes or ratchet retention tightness will be considered.

We present a novel test bed for evaluating helmet fit, dynamic retention, and the effects of both on biomechanical measures of head and neck injury. The presented methods are capable of detecting significant alterations in fit forces, relative head helmet motion, and all the contemporary biomechanical measures of head and neck injury. The proposed methods were used to investigate a regular and backward fit, finding significant changes in head angular velocity and the amount of head exposure. With these proposed methods, distinct differences in helmet performance due to helmet fit can be revealed.

Disclosures

The authors have no conflicts to disclose and do not stand to gain financially from the publication of this work.

Copyright © 2017 Journal of Visualized Experiments

Acknowledgements

We gratefully acknowledge funding from the Natural Science and Engineering Research Council (NSERC) of Canada (Discovery Grants 435921), the Pashby Sport Safety Fund (2016: RES0028760), the Banting Research Foundation (Discovery Award 31214), NBEC Inc. (Canada), and the Faculty of Engineering and Department of Mechanical Engineering at the University of Alberta.

References

1. Thompson, D. C., Rivara, F. P., & Thompson, R. S. Effectiveness of Bicycle Safety Helmets in Preventing Head Injuries: A Case-Control Study. *JAMA*. **276** (24), 1968-1973 (1996).
2. Cripton, P. A., Dressler, D. M., Stuart, C. A., Dennison, C. R., & Richards, D. Bicycle helmets are highly effective at preventing head injury during head impact: Head-form accelerations and injury criteria for helmeted and unhelmeted impacts. *Accid. Anal. Prev.* **70**, 1-7 (2014).
3. Lee, R. S., Hagel, B. E., Karkhaneh, M., & Rowe, B. H. A systematic review of correct bicycle helmet use: how varying definitions and study quality influence the results. *Inj. Prev.* **15** (2), 125-131 (2009).
4. Chang, L.-T., Chang, C.-H., & Chang, G.-L. Fit effect of motorcycle helmet - A finite element modeling. *JSME Int. J. Ser. Solid Mech. Mater. Eng.* **Vol.44** (No.1), 185-192 (2001).
5. Jadischke, R. Football helmet fitment and its effect on helmet performance. *Wayne State Univ. Theses*. at <http://digitalcommons.wayne.edu/oa_theses/176> (2012).
6. Klug, C., Feist, F., & Tomasch, E. Testing of Bicycle Helmets for Preadolescents. *IRCOBI Conf. Proc.* at <https://trid.trb.org/view.aspx?id=1370437> (2015).
7. McIntosh, A. S., & Lai, A. Motorcycle Helmets: Head and Neck Dynamics in Helmeted and Unhelmeted Oblique Impacts. *Traffic Inj. Prev.* **14** (8), 835-844 (2013).
8. Olivier, J., & Creighton, P. Bicycle injuries and helmet use: a systematic review and meta-analysis. *Int. J. Epidemiol.* **46** (1), 278-292 (2017).
9. Rivara, F. P., Thompson, D. C., & Thompson, R. S. Epidemiology of bicycle injuries and risk factors for serious injury. *Inj. Prev.* **3** (2), 110-114 (1997).
10. Ellena, T., Subic, A., Mustafa, H., & Pang, T. Y. The Helmet Fit Index - An intelligent tool for fit assessment and design customisation. *Appl. Ergon.* **55**, 194-207 (2016).
11. Takhounts, E. G., Craig, M. J., Moorhouse, K., McFadden, J., & Hasija, V. Development of Brain Injury Criteria (BrIC). *Stapp Car Crash J.* **57**, 243-266 (2013).
12. Eppinger, R., Sun, E., *et al. Development of improved injury criteria for the assessment of advanced automotive restraint systems - II.* (1999).
13. Mertz, H. J., Irwin, A. L., & Prasad, P. Biomechanical and scaling bases for frontal and side impact injury assessment reference values. *Stapp Car Crash J.* **47**, 155 (2003).
14. Newman, J. A., Beusenberg, M. C., Shewchenko, N., Withnall, C., & Fournier, E. Verification of biomechanical methods employed in a comprehensive study of mild traumatic brain injury and the effectiveness of American football helmets. *J. Biomech.* **38** (7), 1469-1481 (2005).
15. CPSC. *Safety Standard for Bicycle Helmets; Final Rule.* (1998).
16. Miller, N. R., Shapiro, R., & McLaughlin, T. M. A technique for obtaining spatial parameters of segments of biomechanical systems from cinematographic data. *J. Biomech.* **13**, 535-547 (1980).
17. Arun, K. S., Huang, T. S., & Blostein, S. D. Least-Squares Fitting of Two 3-D Point Sets. *IEEE Trans. Pattern Anal. Mach. Intell.* **PAMI**- **9** (5), 698-700 (1987).
18. Smith, T. A., Halstead, P. D., McCalley, E., Kebschull, S. A., Halstead, S., & Killeffer, J. Angular head motion with and without head contact: implications for brain injury. *Sports Eng.* **18** (3), 165-175 (2015).
19. Butz, R., & Dennison, C. In-fibre Bragg grating impact force transducer for studying head-helmet mechanical interaction in head impact. *J. Light. Technol.* **33** (13), 8 (2015).
20. Butz, R. C., Knowles, B. M., Newman, J. A., & Dennison, C. R. Effects of external helmet accessories on biomechanical measures of head injury risk: An ATD study using the HYBRIDIII headform. *J. Biomech.* **48** (14), 3816-3824 (2015).
21. Dennison, C. R., & Wild, P. M. Superstructured fiber-optic contact force sensor with minimal cosensitivity to temperature and axial strain. *Appl. Opt.* **51**, 1188-1197 (2012).
22. Dennison, C. R., & Wild, P. M. Sensitivity of Bragg gratings in birefringent optical fibre to transverse compression between conforming materials. *Appl. Opt.* **49**, 2250-2261 (2010).
23. Knowles, B. M., Yu, H., & Dennison, C. R. Accuracy of a Wearable Sensor for Measures of Head Kinematics and Calculation of Brain Tissue Strain. *J. Appl. Biomech.* **33** (1), 2-11 (2017).
24. Nightingale, R. W., McElhaney, J. H., Richardson, W. J., & Myers, B. S. Dynamic responses of the head and cervical spine to axial impact loading. *J. Biomech.* **29**, 307-318 (1996).
25. Padgaonkar, A. J., Krieger, K. W., & King, A. I. Measurement of Angular Acceleration of a Rigid Body Using Linear Accelerometers. *J. Appl. Mech.* **42** (3), 552-556 (1975).
26. SAE. *J211 Instrumentation for Impact Test - Part 1: Electronic Instrumentation.* **Society of Automotive Engineers.** (2014).
27. Depreitere, B., Lierde, C. V., *et al.* Bicycle-related head injury: a study of 86 cases. *Accid. Anal. Prev.* **36**, 561-567 (2004).
28. Fahlstedt, M., Baeck, K., *et al.* Influence of Impact Velocity and Angle in a Detailed Reconstruction of a Bicycle Accident. *Proc. 2012 Int. IRCOBI Conf. Biomech. Impacts.* 787-799 at <https://lirias.kuleuven.be/handle/123456789/357473> (2012).
29. Newman, J. A. A Generalized Model for Brain Injury Threshold (GAMBIT). *IRCOBI Conf. Proc.* (1986).
30. Newman, J. A., Shewchenko, N., & Welbourne, E. A proposed New Biomechanical head injury assessment function - the maximum power index. *Stapp Car Crash J.* **44**, 215-47 (2000).
31. *Standard Test Method and Equipment used in Evaluating the Performance Characteristics of Protective Headgear/Equipment NOCSAE Doc (ND) 001- 11m12.* (2012).
32. Cobb, B. R., MacAlister, A., Young, T. J., Kemper, A. R., Rowson, S., & Duma, S. M. Quantitative comparison of Hybrid III and National Operating Committee on Standards for Athletic Equipment headform shape characteristics and implications on football helmet fit. *Proc. Inst. Mech. Eng. Part P J. Sports Eng. Technol.* **229** (1), 39-46 (2015).

Copyright © 2017 Journal of Visualized Experiments

33. Cobb, B. R., Zadnik, A. M., & Rowson, S. Comparative analysis of helmeted impact response of Hybrid III and National Operating Committee on Standards for Athletic Equipment headforms. *Proc. Inst. Mech. Eng. Part P J. Sports Eng. Technol.* **230** (1), 50-60 (2016).
34. de Jager, M., Sauren, A., Thunnissen, J., & Wismans, J. Global and a Detailed Mathematical Model for Head-Neck Dynamics. *Proc. Stapp Car Crash Conf.* **40**, 269-281 (1996).
35. Aare, M., & Halldin, P. A New Laboratory Rig for Evaluating Helmets Subject to Oblique Impacts. *Traffic Inj. Prev.* **4** (3), 240-248 (2003).